

Fig. 2. Porous Ni corrosion rates in  $\text{Ni}(\text{NO}_3)_2$  solution

into the heated solution for the prescribed time, washed thrice in 60°C DI water, and dried at 115°C for 30 min in a forced air oven.

Nitrate solutions were 5.4M  $\text{Ni}(\text{NO}_3)_2$  using reagent grade material and were maintained at 80°C. The nitrate solutions free  $\text{HNO}_3$  concentration was maintained at  $5 \times 10^{-2}\text{M}$   $\text{HNO}_3$ , unless otherwise noted, as determined by a NaOH titration to a methyl red indicator end point.

### Results and Discussion

Table I lists the porous Ni plaque corrosion rates determined by the above-outlined technique for plaque passivated prior to nitrate solution exposure. The corrosion rates show the expected result, i.e., the formation of an oxide on the Ni surface greatly reduces the solution corrosion level. This is consistent with the acidic dissolution reaction given in Eq. [1] and the fact that NiO is considerably more stable in mild  $\text{HNO}_3$  solution than metallic Ni. Somewhat surprising, however, is the observation that the corrosion rates for thermally passivated samples are somewhat lower than those obtained for samples which have been chemically passivated in strong oxidizing solutions. This result occurs in spite of the fact that thermally passivated substrates possess a thicker oxide coating as deter-

mined both visibly by the plaque color change from gray to pale green or gold, and also by Auger electron spectroscopy coupled with  $\text{Ar}^+$  milling. The reasoning for this rate differential may be found in the morphological characteristic of the oxide formed by these two techniques. No chemical differences were found between the oxides grown by the two techniques. Thermally grown oxide scale, even for thin coatings such as seen here, possess a multigranular structure. This structure results when the outward growing oxide scale fractures, since the stresses induced by the rapid oxide growth rate and volume change exceed the flexure strength of the oxide. The result of this fracture, for thin films, is the presence of pores and fractures in the coating which expose areas of Ni covered by only a very thin oxide film. The resulting nodular oxide film structure is seen in Fig. 1a; a considerably more uniform and dense oxide surface resulting from chemical passivation is seen in Fig. 1b. In either case, however, the formed oxide surface protects the interior Ni layer from corrosive attack during solution contact.

The effectiveness of chemical passivation in reducing Ni plaque corrosion in this system is seen in Fig. 2. Here the porous Ni plaque corrosion rate is presented for two different  $\text{HNO}_3$  concentrations within the  $\text{Ni}(\text{NO}_3)_2$  solution. If the reduction in Ni corrosion rate is assumed proportional to the passivating oxide coverage, the results show an initially rapid oxide formation followed by a slower sustained growth rate. This leads to approximately an order-of-magnitude reduction in Ni plaque corrosion rate following a 20 min exposure to the 95°C, 2M  $\text{K}_2\text{Cr}_2\text{O}_7$  solution. In absolute terms, these data mean the following for a solution impregnated under the higher of the two  $\text{HNO}_3$  concentrations. An unpassivated Ni plaque, given a 10 min  $\text{Ni}(\text{NO}_3)_2$  impregnation, would lose 8.2% of its total Ni content to corrosion, whereas the same plaque passivated for 30 min in the 95°C  $\text{K}_2\text{Cr}_2\text{O}_7$  solution would experience a Ni loss of only 0.6%. The electrode's Ni fiber strength following impregnation was shown previously to be inversely proportional to the extent of plaque corrosion (1), therefore the reduced corrosion occurring with passivated substrates is expected to significantly improve both the electrode's handling characteristics during cell winding and its cycle life.

### Acknowledgment

The author acknowledges fruitful discussions with personnel at Gates Energy Products, Incorporated, Gainesville, Florida.

Manuscript submitted Sept. 27, 1987; revised manuscript received March 4, 1988.

General Electric Company assisted in meeting the publication costs of this article.

### REFERENCES

1. C. E. Baumgartner, *This Journal*, **135**, 36 (1988).
2. A. Fleischer, *Trans. Electrochem. Soc.*, **94**, 289 (1948).
3. E. J. Casey, P. L. Bourgault, and P. E. Lake, *Can. J. Technol.*, **34**, 95 (1956).
4. J. L. Weininger, in "The Nickel Electrode," R. G. Gunther and S. Gross, Editors, p. 1, The Electrochemical Society Softbound Proceedings Series, PV 82-4, Pennington, NJ (1982).
5. R. T. Barton, P. J. Mitchell, and N. A. Hampson, *Surf. Coat. Tech.*, **28**, 1 (1986).

## Reactivity of Porous Graphite in Chlorinated Acidic Solution

Jacob Jorne, Emad Roayaie,\* and Shyam Argade\*\*

Department of Chemical Engineering, University of Rochester, Rochester, New York 14627

Graphite has been used for anodes in both the chlor-alkali and chlor-acidic cells. The desirable characteristics

\* Present address: National Iranian Oil Company, Research Center, Tehran, Iran.

\*\* Present address: Technochem Company, Winston-Salem, North Carolina 27101.

such as low resistivity, machineability, satisfactory chlorine overpotential, and finally, resistivity to chemical attack makes graphite the proper material. Graphite wear in chlor-alkali systems was investigated by Marek and Heintz (1). Their studies included the effect of structural parameters on the wear of graphite anode. Rabah *et al.* (2) investi-

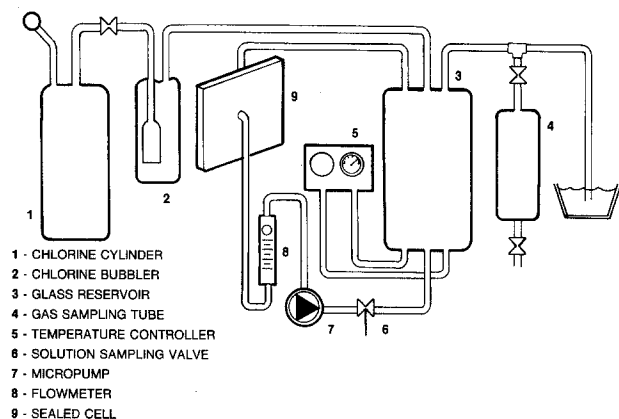
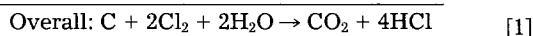


Fig. 1. Experimental setup for the degradation measurement

gated the wear of graphite anodes during electrolysis of acid sulfate solutions. They studied the effect of parameters such as, temperature, acid concentration, pH, and also current density on the graphite wear. They concluded that formation of an unstable lamellar crystal compound is responsible for the graphite corrosion at low temperatures. However, in acidic media such as in the operation of the zinc-chloride battery, a degradation of the porous-graphite electrode has been observed in the form of evolved carbon dioxide gas. The evolution of  $\text{CO}_2$  can be attributed to chemical and electrochemical mechanisms. The electrochemical degradation mechanisms of porous graphite is the subject of the present discussion.

#### Postulated Mechanism

It is postulated that the electrochemical deterioration of porous graphite in chlor-acidic media follows a local action mechanism



Separate study of the half reactions would generate enough data for the polarization curves from which the corrosion current and potential values could be determined. In the present study, the rates of  $\text{CO}_2$  and HCl formation are determined and compared to the postulated local-action mechanism.

#### Experimental Procedure

According to the postulated mechanism, the rate of HCl formation should be four times the rate of  $\text{CO}_2$  evolution.

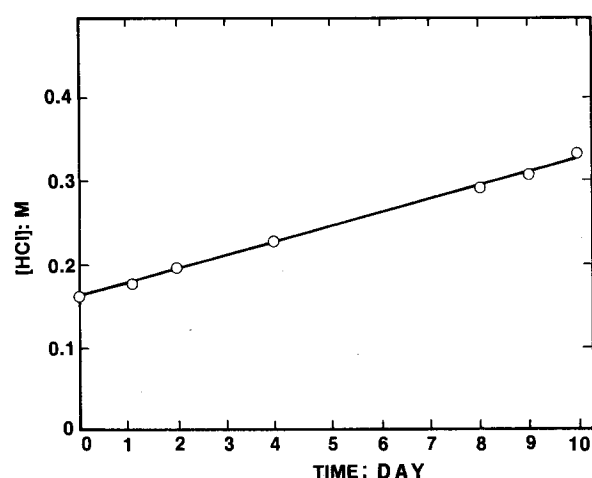


Fig. 2. Cumulative generation of HCl with time

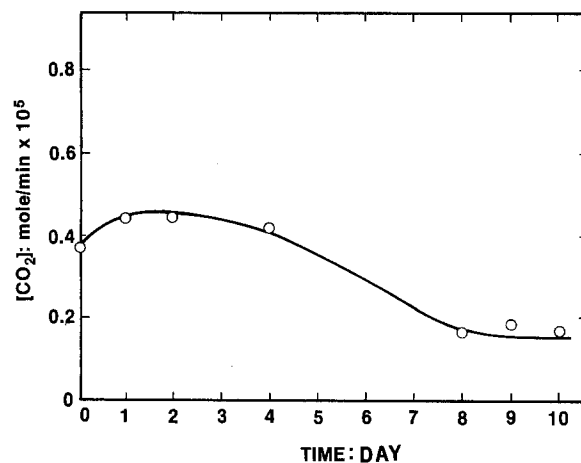


Fig. 3. Rate of  $\text{CO}_2$  evolution with time

In order to verify this mechanism, the following experimental apparatus has been assembled in which both the evolution of  $\text{CO}_2$  and the concentration of  $\text{H}^+$  are being measured simultaneously. The experimental apparatus is shown in Fig. 1. It consisted of a flow-through cell in which chlorinated HCl electrolyte was circulated through a porous graphite plate.

The temperature was controlled by circulating water through a hot bath maintained at  $80^\circ\text{C}$ . The  $\text{H}^+$  concentration was measured by titration with sodium hydroxide. Periodically,  $10\text{ cm}^3$  samples were taken, dechlorinated quickly by nitrogen bubbling, and were titrated by  $0.1\text{N}$  NaOH solution. The rate of  $\text{CO}_2$  evolution was measured by a gas chromatograph.

#### Results and Discussion

The plot of HCl concentration over a period of 10 days is shown in Fig. 2 and the rate of  $\text{CO}_2$  evolution is plotted in Fig. 3. It should be noted that the HCl concentration is a cumulative plot; therefore, a comparison between the two graphs should be done by integrating the rate of  $\text{CO}_2$  evolution over the time of the experiment. The amount of  $\text{CO}_2$  evolved during a 10-day period was calculated by integrating Fig. 3

$$\text{CO}_2 = 4.75 \times 10^{-2} \text{ mol} \quad [2]$$

The amount of HCl can be read directly from Fig. 2, after correcting for changes in the volume of the circulated solution. The amount of HCl formed =  $(0.34\text{M} \times 1.15 \text{ liter}) - (0.162\text{M} \times 1.09 \text{ liter}) = 0.214 \text{ mol}$ . The corresponding average rates are

$$\bar{r}_{\text{CO}_2} = 0.33 \times 10^{-5} \text{ mol/min} \quad \bar{r}_{\text{HCl}} = 1.49 \times 10^{-5} \text{ mol/min} \quad [3]$$

The experimental results strongly indicate that the rate of HCl formation is four times the rate of  $\text{CO}_2$  evolution, in agreement with the postulated mechanism. The amount of carbon loss over a 10-day period is roughly  $0.5\text{g}$ , or about 3-4% of the original weight of the graphite sample. The significant losses can account for changes in surface area and pore size distribution.

The trend in the  $\text{CO}_2$  evolution over the period of the experiment (Fig. 3) may be another evidence to show that the graphite degradation mechanism follows the local corrosion reaction. In acidic solutions, dissolved chlorine attacked the active sites on the graphite surface both through chemical and electrochemical reactions. Initially, the electrode contained many blocked pockets with their areas only exposed to the anodic reaction. Therefore, the reaction was initially limited by the cathodic reduction of chlorine. As chlorine-saturated solution flowed through the open pores, chlorine reacted with graphite at the active sites. Closed pockets were gradually opened and the cathodic area for the chlorine reduction increased (see maximum in Fig. 3).

As the experiment proceeded, active sites became covered by the surface oxides due to the chemical corrosion of graphite [Suidan *et al.* (3)] which is responsible for the decline in the rate of CO<sub>2</sub> evolution in Fig. 3. Finally, a steady state was reached where the rate of CO<sub>2</sub> evolution remained unchanged.

#### Acknowledgments

This work was jointly supported by Energy Development Associates (Gulf and Western Company) and the Electric Power Research Institute.

Manuscript received July 6, 1987.

#### REFERENCES

1. R. W. Marek and E. H. Heintz, "Effect of Macropore Surface Area on Graphite Anode Wear in Laboratory Test Cell," Airco-Speer Carbon Graphite, Technical Department, P.O. Box 828, Niagara Falls, NY 14302.
2. M. A. Rabah, A. A. Abdal Azim, and A. Ismail, *J. Appl. Electrochem.*, **11**, 41 (1981).
3. M. T. Suidan, V. L. Snoeyink, and R. A. Schmitz, *Environ. Sci. Technol.*, **VII**, 785 (1977).

## Methane Activation to C<sub>2</sub> Hydrocarbon Species in Solid Oxide Fuel Cell

Nirupama U. Pujare and Anthony F. Sammells\*

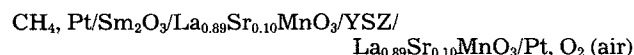
Eltron Research, Incorporated, Aurora, Illinois 60504

Methane electrochemical oxidation to CO<sub>2</sub> and H<sub>2</sub>O in the anode compartment of a solid oxide fuel cell (SOFC), after its initial steam reformation to hydrogen, is a strategy currently being developed for the direct conversion of natural gas into dc electricity. Methane, however, is also an important chemical feedstock from which the commercially more valuable C<sub>2</sub> hydrocarbon species C<sub>2</sub>H<sub>4</sub>, C<sub>2</sub>H<sub>2</sub>, and C<sub>2</sub>H<sub>6</sub> might be produced. This latter goal could, in principle, be achieved by the partial electrochemical oxidation of methane using appropriate anode electrocatalysis for the SOFC.

Previous workers (1) have investigated the influence of mediated O<sup>2-</sup> species through the oxygen-conducting solid electrolyte yttria stabilized zirconia (YSZ) on heterogeneous gas phase methane oxidative dimerization reactions leading to C<sub>2</sub> species. Using the cell Ag, MgO/YSZ/Ag, passage of CH<sub>4</sub> and O<sub>2</sub> mixtures through the Ag, MgO anode compartment under open-circuit conditions at 700°C gave trace C<sub>2</sub>H<sub>4</sub> and C<sub>2</sub>H<sub>6</sub>. Upon electrochemically driving O<sup>2-</sup> through the cell to the Ag, MgO anode, C<sub>2</sub>H<sub>4</sub> yield was found to dramatically decrease with C<sub>2</sub>H<sub>6</sub> being unaffected. In comparison, other workers (2) using the cell Ag, Bi<sub>2</sub>O<sub>3</sub>/YSZ/Ag showed that methane oxidative dimerization, mainly to C<sub>2</sub>H<sub>6</sub>, could be promoted when only faradaically driven oxygen was available at the Ag, Bi<sub>2</sub>O<sub>3</sub> anode.

Several rare earth metal oxides (3), including Sm<sub>2</sub>O<sub>3</sub>, have been shown to be active sites for promoting chemical methane oxidative dimerization from CH<sub>4</sub>/O<sub>2</sub> mixtures. C<sub>2</sub> selectivities up to 95% were reported. The high activity of these rare earth oxides appeared related to their ability for accommodating populations of surface O<sup>-</sup> species. The above observations encouraged us to investigate anode electrocatalytic sites which incorporated rare earth metal oxides, for promoting faradaic methane oxidative dimerization to C<sub>2</sub> hydrocarbons.

The fuel cell investigated possessed the general configuration



and used a closed-one-end YSZ solid electrolyte tube. La<sub>0.89</sub>Sr<sub>0.10</sub>MnO<sub>3</sub> electrodes were introduced into both the anode and cathode regions of the SOFC by applying a 5 w/o suspension in ethylene glycol/citric acid of La(C<sub>2</sub>H<sub>3</sub>O<sub>2</sub>), SrCO<sub>3</sub>, and MnCO<sub>3</sub> of appropriate composition onto both the outside and inside walls of the YSZ tube. Current collection from each of these regions was via platinum wire (0.25 mm) initially in close mechanical contact to the YSZ. Decomposition of the electrocatalyst precursor was achieved by heating the tube assembly to 800°C in air for

1h followed immediately by heating the cell assembly to 1250°C for 1h to form the La<sub>0.89</sub>Sr<sub>0.10</sub>MnO<sub>3</sub> electrodes. Samaria (Sm<sub>2</sub>O<sub>3</sub>) was introduced as a thin layer suspension in DMF onto the inside wall anode surface of the fuel cell. Estimated Sm<sub>2</sub>O<sub>3</sub> loading was 20 mg/cm<sup>2</sup>. The assumption was made that upon heating the cell to ≈900°C, some limited sintering or solid-state diffusion by Sm<sub>2</sub>O<sub>3</sub> into La<sub>0.89</sub>Sr<sub>0.10</sub>MnO<sub>3</sub> may occur at their interface. However, we suspect that diffusion by Sm<sub>2</sub>O<sub>3</sub> into perovskite sites would be localized and not result in significant changes to the bulk properties of either these two materials.

Anode fuel gas typically comprised 10% CH<sub>4</sub> in argon. At 760°C the cell possessed an open-circuit potential (OCP) of 1.25V. The cathode oxygen source was air. Analysis of anode reaction products was performed using a GOWMAC Model 69-750 FID gas chromatograph using a 6 ft × 1/8 in. stainless steel column packed with 80/100 mesh Carbosphere (Alltech Associates, Incorporated). No C<sub>2</sub> species were evident from either the methane or argon sources used in this work.

Initial measurements were performed under OCP conditions with O<sub>2</sub> being intentionally introduced into CH<sub>4</sub>/Ar

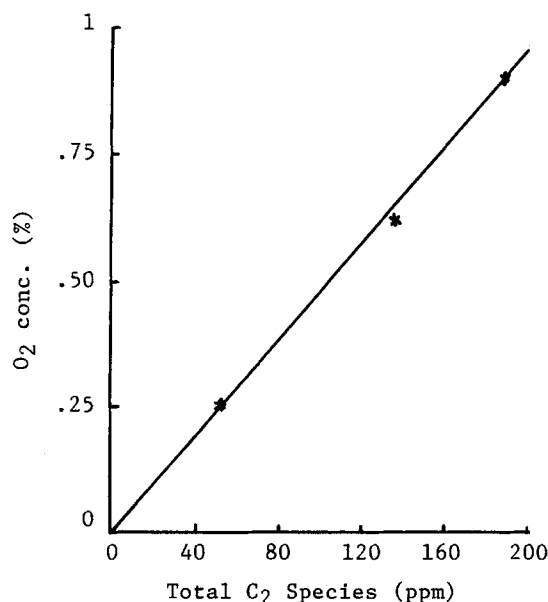


Fig. 1. Oxygen concentration (%) vs. total C<sub>2</sub> species (C<sub>2</sub>H<sub>2</sub> + C<sub>2</sub>H<sub>4</sub> + C<sub>2</sub>H<sub>6</sub>) under OCP conditions for the cell CH<sub>4</sub>, Pt/Sm<sub>2</sub>O<sub>3</sub>/La<sub>0.89</sub>Sr<sub>0.10</sub>MnO<sub>3</sub>/YSZ/La<sub>0.89</sub>Sr<sub>0.10</sub>MnO<sub>3</sub>/Pt, O<sub>2</sub> (air). Initial OCP 1.23V. Anode gas comp. 10% CH<sub>4</sub>, O<sub>2</sub>, Ar (balance). Flow rate 50 ml/min. Temperature 760°C.

\*Electrochemical Society Active Member.